J. Fluid Mech. (1986), *vol.* 162, *pp.* 389–413
Printed in Great Britain

Burst detection with single-point velocity measurements

By D. G. BOGARD† AND W. G. TIEDERMAN
School of Mechanical Engineering, Purdue University,
W. Lafayette, Indiana 47907 U.S.A.

(Received 13 December 1984)

An evaluation of the effectiveness of the VITA, Quadrant, TPAV, *U*-level, Positive slope, and VITA with slope burst-detection algorithms has been done by making direct comparisons with flow visualization. Measurements were made in a water channel using an X-type hot-film probe located in the near-wall region. Individual ejections from bursts which contacted the probe were identified using dye flow visualization. The effectiveness of each of the detection algorithms was found to be highly dependent on the operational parameters, i.e. threshold levels and averaging or window times. These parameters were adjusted so that the number of events detected by each of the algorithms corresponded to the number of ejections identified by flow visualization, while the probability of a false detection was minimized. Comparing the detection algorithm using these optimum parameter settings, the Quadrant technique was found to have the greatest reliability with a high probability of detecting the ejections and a low probability of false detections. Furthermore, it was found that the ejections detected by the Quadrant technique could be grouped into bursts by analysing the probability distribution of the time between ejections.

1. Introduction

In the flow-visualization studies by Kline *et al.* (1967) it was established that important characteristics of the near-wall region of bounded turbulent flows are the low-velocity streaks in the sublayer, and the subsequent ejection of the low-velocity fluid to the outer region of the flow. Quantitative analyses of flow-visualization studies by Corino & Brodkey (1969), Kim, Kline & Reynolds (1971), and Grass (1971) indicated that the ejection of low-velocity fluid from the wall region was associated with a major part of the Reynolds stress and turbulent-energy production. These results provided a strong impetus for further studies aimed at understanding the dynamics of the ejection process and its association and interaction with the large-scale structure in turbulent boundary layers.

There are several stages in the process by which the fluid in a low-velocity streak is eventually ejected away from the wall. The total process was called a 'burst' by Kim *et al.* (1971) and the following paraphrases their description of the bursting process. Initially the low-velocity streak slowly lifts away from the wall, at which time the streak filament begins to oscillate in both the spanwise and normal directions. The burst process continues as the loops of the streak filaments eject away from the wall. Finally, as the streak filaments eject away from the wall they eventually break up in a chaotic process. Although each of these processes is not always distinguishable

† Present address: Mechanical Engineering Department, University of Texas at Austin.

in each burst, the burst is always associated with the ejection of fluid away from the wall. Furthermore, as noted by Offen & Kline (1975), a burst may involve only one ejection or several ejections closely grouped together.

Although flow-visualization studies have been effective in giving a general description of the burst, it is apparent that flow-visualization techniques have neither the capability for extensive quantitative measurements nor the range in Reynolds number necessary to determine details of the burst event such as the appropriate scaling. Consequently many studies have been performed using probes with the intention of measuring the velocity and pressure fields associated with bursts. Given a reliable detection algorithm, probe measurements can be made at much higher Reynolds numbers than is possible with flow visualization. Probe measurements have an additional advantage with the capability of using conditional sampling to educe average-velocity characteristics occurring during the bursting process.

As mentioned above, the key to using probe measurements is the availability of a reliable method for identifying bursts with velocity or pressure measurements. Numerous methods have been proposed and used. The first of these was a short-time autocorrelation used by Kim *et al.* (1971). The autocorrelation is intended to measure the average time between bursts $\overline{T}_{\mathrm{B}}$ but is not capable of detecting individual events. Using this technique Kim *et al.* found that the first positive peak in the autocorrelation, although small in magnitude, had a lag time which corresponded well with the $\overline{T}_{\mathrm{B}}$ value obtained from flow visualization.

Several techniques for detecting individual events, bursts or ejections, have been developed based on the observation by Kim *et al.* (1971) that the break-up of the ejected fluid was very chaotic. Rao, Narasimha & Badri Narayanan (1971) used the band-pass-filtered velocity signal to detect time periods when the streamwise velocity was highly energetic. Blackwelder & Kaplan (1976) used variable-interval time averaging (VITA) to detect large variances in the streamwise-velocity signal. Chen & Blackwelder (1978) added a slope condition to the VITA technique so that only events with rapid accelerations in the streamwise velocity component would be detected. Previously Simpson (1976) had used only a large positive slope in the velocity signal to detect events.

Other velocity-signal characteristics have also been used for burst detection. Lu & Willmarth (1973) used two detection techniques: one based on the magnitude of the streamwise velocity being below a certain threshold; and the other based on the magnitude of the second quadrant uv product (i.e. when u is negative and v is positive). Here u and v are respectively the turbulent fluctuations about the mean velocity components in the streamwise direction x and the direction normal to the wall y. Wallace, Brodkey & Eckelmann (1977) used a pattern-recognition technique to identify events starting with a negative gradient in the streamwise velocity, followed by a positive gradient that was greater in magnitude than the preceding negative gradient.

Each of these detection algorithms is based on a velocity-signal pattern that is postulated to be a unique characteristic of bursts. However, discrepancies are quite evident when comparing the results obtained from the different techniques in making the fundamental measurement of $\overline{T}_{\mathrm{B}}$. These results are presented in figure 1 for fully developed channel and pipe flows, and in figure 2 for zero-pressure-gradient boundary layers. The wide scatter in the results is indicative that the number of bursts detected per unit time varies significantly depending on which detection algorithm is used. Normalization has been done with outer variables, which are the centreline velocity U_0 and channel half-width or pipe radius h in figure 1, and free-stream velocity U_∞

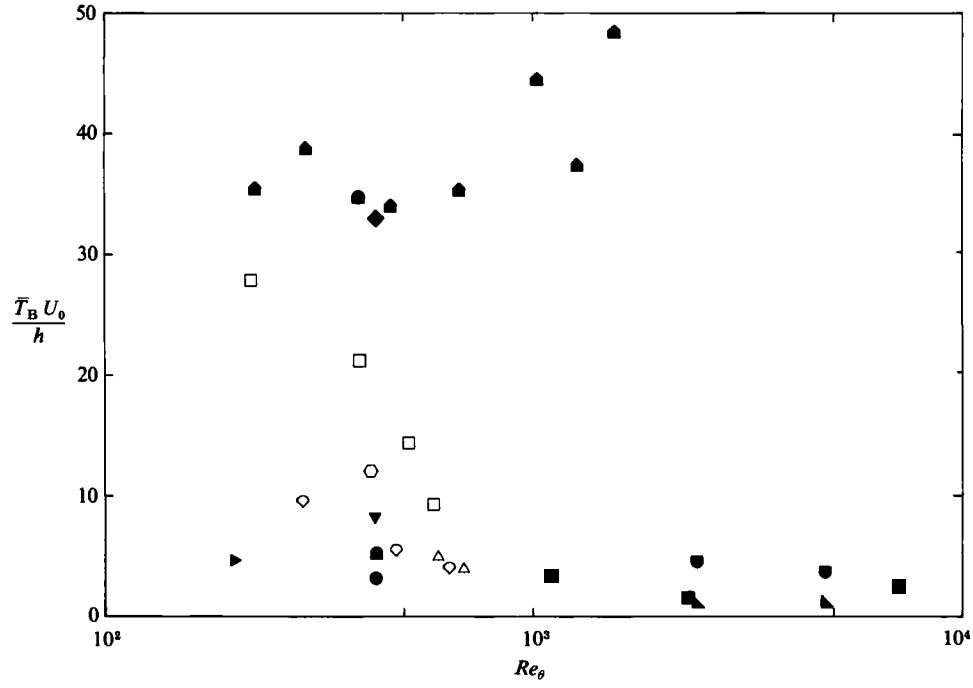

FIGURE 1. Average bursting periods for channel and pipe flows: open symbols, visual; closed symbols, probe. ○, present; □, Donohue, Tiederman & Reischman (1972); △, Tiederman *et al.* (1977); ▽, Achia & Thompson (1977); ▶, Ueda & Mizushina (1977); ▲, Mizushina & Usui (1977); ■, Heidrick, Banerjeee & Azad (1977); ⛊, Sabot & Comte-Bellot (1976); ◣, Comte-Bellot *et al.* (1978). Oil-channel investigations: ◆, Blackwelder & Eckelmann (1977); ▼, Simpson (1976); ⬢, Wallace *et al.* (1977); ●, Brodkey *et al.* (1974).

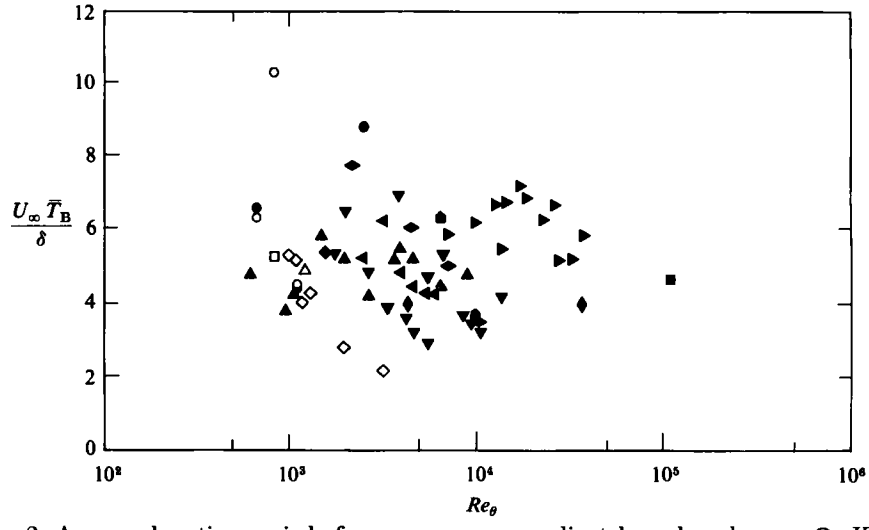

FIGURE 2. Average bursting periods for zero-pressure-gradient boundary layers: ○, Kim *et al.* (visual) (1971); △, Smith (1978); ◇, Kline *et al.* (1967); □, Offen & Kline (ejections) (1975); ⬭, Offen & Kline (bursts) (1975); ◆, Blackwelder & Haritonidis (1983); ▲, Willmarth & Sharma, 1984; ●, Kim *et al.* (probe) (1971); ▲, Rao *et al.* (1971); ◆, Kasagi & Hirata (1976); ▼, Strickland & Simpson (1975); ◀, Laufer & Narayan (1971); ▶, Narayan & Martin (1978); ⧫, Lu & Willmarth (1973); ■, Zakkay, Barra & Wang (1978); ⬢, Blackwelder & Kaplan (1976).

and boundary-layer thickness δ in figure 2. In both cases the momentum-thickness Reynolds number Re_θ is based on the maximum local velocity (U_0 or U_∞). Similar results are obtained when normalizing with inner variables (Bogard & Tiederman 1983). This fundamental question of the appropriate scaling for the time between bursts is still unresolved. Even investigators using the same method for detecting bursts (Blackwelder & Haritonidis 1983; and Alfredsson & Johansson 1984) recently have reached different conclusions regarding the appropriate scaling.

Of particular interest in figure 1 are the results of Brodkey, Wallace & Eckelmann (1974), Wallace *et al.* (1977), Simpson (1976), and Blackwelder & Eckelmann (1977) who all performed experiments in the same oil-channel facility with the same flow conditions ($Re_\theta = 400$). However, each used different burst-detection algorithms with their velocity measurements. The order-of-magnitude variation in $\overline{T}_B$ obtained in these four investigations must be attributed solely to differences in the detection algorithms used to analyse the velocity signals.

For each of the detection algorithms discussed above, a threshold level must be established for when the signal characteristic is strong enough to indicate a burst. Ideally one would expect that the number of events detected would be insensitive to the threshold over some finite range. However, all of these detection algorithms have a monotonically decreasing number of detections with increasing threshold. Consequently, the appropriate threshold level for each of the algorithms cannot be determined without some ambiguity.

Recognizing this fact, recent investigations using the VITA technique (Blackwelder & Haritonidis 1983) and the Quadrant technique (Raupach 1981) have noted that their results should be interpreted in terms of qualitative trends rather than exact numerical values for $\overline{T}_B$. Nakagawa & Nezu (1981) compensated for the ambiguity of the threshold level by using weighting factors, dependent on threshold, for conditional-sampling studies. Events detected at high thresholds, and thus more likely to be valid, were weighted more heavily than events detected at lower thresholds.

Besides the uncertainty regarding the appropriate threshold for each of the detection algorithms, there is generally no consideration given to whether the algorithm is detecting a single ejection or the total burst event. Since a burst can have several ejections, there would be a large difference in timescales depending on whether ejections or bursts are detected.

The most fundamental question to be addressed for any detection algorithm is whether the signal characteristics used for the detection are actually unique characteristics of an ejection or burst. That is, do the detection algorithms reliably detect either ejections or bursts? To resolve the question, Offen & Kline (1975) made a direct comparison between various detection algorithms and dye flow visualization of ejections. The conclusion of that study was that there was no significant correlation between the flow visualization and any of the velocity-detection algorithms. However, according to the results of Bogard & Tiederman (1983), Offen & Kline placed their probe at a streamwise position relative to the dye slot, $x^+ = 240$, where a large percentage of the bursts are not marked by the dye flow visualization.† Hence the poor correspondence between the flow visualization and the burst-detection algorithms obtained by Offen & Kline was not conclusive.

Clearly there is a need for a thorough evaluation of the various detection algorithms

† The superscript + indicates that the variable has been made dimensionless using the kinematic viscosity ν and the wall shear velocity $u_\tau = \tau_w/\rho$.

to resolve the discrepancies between the techniques, to determine appropriate threshold levels, and to establish the validity of each of the techniques via direct comparison with flow visualization. In the present investigation this evaluation has been done by comparing various detection techniques with dye flow visualization of ejections. Particular care was taken to ensure that the dye flow visualization reliably and exactly identified all ejections that intersected the probe. The detection algorithms were evaluated in terms of the probability that an ejection will be detected and the probability of a false detection. Operational parameters for the algorithms, including threshold, have been determined so that the probability of a false detection is minimized while maintaining the detection rate equivalent to the number of visually identified ejections. Finally, procedures are presented for educing burst events from the detection of individual ejections made with a probe.

2. Experimental details

2.1. *Facilities*

Experiments were conducted in the fully developed turbulent flow of a two-dimensional water channel. A schematic of the facility is shown in figure 3. The channel had an internal cross-sectional dimension of 60 × 575 mm, was 4.93 m in length, and was constructed of $\frac{1}{2}$ in. Plexiglas. An upstream stilling tank contained a perforated plate, screens and foam to ensure a smooth, uniform flow at the entrance to the channel. Another stilling tank at the downstream end of the channel ensured that disturbances from the recirculating piping system were not propagated upstream into the channel. A cooling coil was installed in the downstream stilling tank for temperature control of the water. The flow entered the channel through a smooth two-dimensional contraction and then passed through a flow straightener composed of plastic drinking straws. The effectiveness of the flow-management system was checked using dye and hydrogen-bubble flow visualization and the existence of a smooth and uniform flow at the inlet was verified.

Two $1\frac{1}{2}$ horsepower pumps recirculated the water with a maximum mean velocity for the channel of approximately 0.3 m/s. Measurement of flow rate was made with an orifice flowmeter installed in the return piping and calibrated in-line. Three static pressure taps were built into the channel starting from 2.0 m downstream of the inlet and spaced at intervals of 1.3 m. Differential pressures were measured with a micrometer manometer, which had a sensitivity of 0.015 mm of water when carbon tetrachloride was used as the manometer fluid.

2.2. *Flow visualization*

A fluorescent dye injected through a dye slot in the bottom wall of the channel was used to mark the wall-layer flow structures. The dye slot was 0.125 mm wide, 200 mm long, and was located 3.7 m downstream of the channel inlet. The downstream distance was more than 60 channel heights, which ensured that the turbulence properties of the flow were fully developed at the dye-slot location. Dye solutions were made from fluorescein disodium salt mixed in concentrations from 4 to 8 g/l of water. Dye was introduced into the channel at a very slow flow rate equal to $\frac{1}{20}$ of the flow rate in the linear sublayer ($y^+ \leqslant 8$) so that the injection process caused no appreciable disturbance to the flow. The flow rate of the dye was monitored using a rotameter flowmeter.

A thin light plane parallel with the flow and normal to the wall was used to illuminate the fluorescent dye. The light plane was formed by constructing two

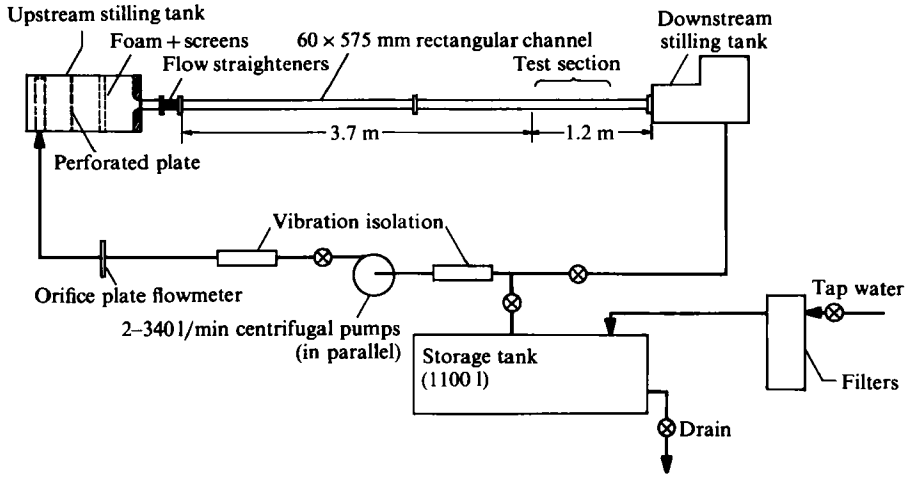

FIGURE 3. Schematic of flow loop.

collimated light sources using 600 watt quartz bulbs and passing the light through two 1.5 mm wide slits. Due to imperfect collimation of the light source, the light plane spread to a width of less than 3 mm at the bottom wall of the channel. Since a fluorescent dye was used, only the dye that was within the light plane was illuminated. Thus, in effect, the light plane revealed a two-dimensional cross-section of the dye-marked three-dimensional structure.

Recordings of the flow visualization were made with a Video Logic Corporation Instar high-speed motion analyser. This black-and-white video system was used at a framing rate of 120 frames/s. Analysis of the video tapes was done using the slow-motion and frame-by-frame modes of playback.

2.3. *Hot-film measurement and recording*

Velocity measurements in the water channel were made using a TSI model 1249-10W miniature hot-film X-probe. Signals were digitized and stored on magnetic tape, and later analysed with a CDC 6600 computer.

The TSI miniature X-probe has two cylindrical hot-film sensors. Each sensor has a diameter of 25 μm and a length of $l = 0.5$ mm, and the spacing between the sensors is 0.5 mm. When normalized with inner variables, the length and spacing between the sensors were $l^+ = 4$. Blackwelder & Haritonidis (1983) determined that this length was sufficiently small to yield accurate measurements of the turbulent structures. The hot-film probe was traversed across the channel using a micrometer with an accuracy of ± 0.025 mm. Two DISA CTA standard 55M10 bridges and DISA 55D10 linearizers were used to operate the hot-film probe. Using the square-wave test, a frequency response of 3 kHz was estimated for the system.

The hot-film probe was calibrated at the centreline of the channel. A Pitot probe connected to the micrometer manometer was used to establish the centreline velocity at various channel-flow rates. These velocity measurements were then used to calibrate the hot-film probe. The yaw constant for the probe was determined using the method of Taslim, Kline & Moffat (1978). Effects due to spanwise velocity fluctuations were neglected based on the observations of Eckelmann (1974) that this would cause less than a 3.5% error in the streamwise velocity and no error in the normal-velocity measurements.

An interface was constructed to digitize the two anemometer signals and to read the data onto a digital magnetic-tape drive. Two channels of data were digitized with 12 bit accuracy and a rate of 70 Hz per channel. This digitizing rate corresponds to an interval between data points of $t^+ = 0.9$. The accuracy of the digitized data was checked by comparing digitized output with the equivalent analog output displayed on an oscilloscope during time periods of high velocity fluctuations; no difference between the two could be discerned.

2.4. *Procedures*

Experiments were conducted in which flow visualization of bursts was done simultaneously with velocity measurements made with the X-film probe. The X-film probe was located at $y^+ = 15$ above the lower wall of the channel and a distance $x^+ = 855$ downstream of the dye slot. At this position, the probe was in the centre of the 'full-detection region' for ejections using dye-slot flow visualization. The 'full-detection region' was shown by Bogard & Tiederman (1983) to be the streamwise region downstream of the dye slot where dye will mark all ejections.

Bogard & Tiederman (1983) also showed that, because of the spanwise oscillation of the lifted streak, the average spanwise width over which an ejection can be detected is $z^+ = 100$. Conequently, for the relatively narrow light plane used in the present study, $z^+ = 23$, the number of ejections visualized was independent of the width of the light plane. In the present study, the light plane was aligned to pass directly through the X-film probe. Since the ejecting streak filament would generally cross the full width of the light plane, essentially all ejections that were illuminated by the light plane also passed through the probe.

Two cameras were used with the video system for these experiments. One camera was used for the flow visualization with a field of view which extended over a range of $x^+ = 400$ upstream of the probe. The second camera was used to project in the corner of the screen the image of a counter that indicated when the hot-film interface was digitizing and storing a data point. By this means the flow-visualization recordings were synchronized with the velocity data.

In the analysis of the flow visualization, individual ejections from a burst were identified using criteria similar to those used by Bogard & Tiederman (1983). In their study, an ejection was defined as an element of dye-marked fluid that originated from within $y^+ = 15$ of the wall and which had a vertical movement beyond $y^+ = 35$ within a distance of $\Delta x^+ = 350$. For the most part these criteria were sufficient for the present study; however, for ejections that originated very close to the probe, a vertical movement of $\Delta y^+ \geqslant 20$ could not be verified owing to flow disturbance caused by the probe. Because of this, the criteria for an ejection were relaxed to include events which originated within $x^+ = 200$ of the probe and had a vertical movement of $\Delta y^+ \geqslant 10$, and events which originated within $x^+ = 100$ of the probe and had a vertical movement of $\Delta y^+ \geqslant 5$.

For each ejection the following information was recorded: time of first contact, time contact ended, streamwise position of the origin, and ejection category. The ejection categories are described in table 1. The first four categories in this table classify the ejections in terms of the stage of development of the ejection when it contacts the probe. Categories 5 and 6 are ejections that mainly pass above the probe and only a trailing tail from these ejections actually contacts the probe. The categories in table 1 are arranged in an order corresponding to the likelihood of having identifiable flow patterns that could be detected by a velocity probe. Ejections in category 1 would be the most likely to be detected, while those in category 6 have a very poor

1. Ejection in the middle stage of development, clearly distinguishable and still strongly lifting (moving away from the near wall) as it passes through the probe.
2. Latter stage of development, clearly distinguishable and still lifting (but not strongly) at the probe.
3. Early stage of development, ejections that originate very close to the probe but are not clearly distinguishable owing to the short distance they can be viewed before they reach the probe.
4. Ejection development has finished upstream of the probe with no apparent lifting when the probe is reached.
5. Head of the ejection passes over the top of the probe with only the tail contacting the probe. The lifting or non-lifting of this tail is ambiguous.
6. Head of the ejection passes over the top of the probe with the tail of the ejection clearly not lifting as it contacts the probe.

TABLE 1. Ejection categories

probability of detection. These characteristics, and other recorded statistics, were manually written into computer files. Subsequent comparisons between flow visualization results and velocity measurements were made using specially written computer programs.

When making hot-film measurements simultaneously with dye injection into the channel, it was critical to ensure that the injected fluid would not cause erroneous velocity measurements due to a difference in temperature. This was accomplished by placing thermocouples in the dye reservoir and in the channel test section, which allowed the temperatures of the two to be matched within 0.2 °F. Effects on the hot-film measurements due to dye injection were also checked by comparing these data with velocity measurements made without dye injection immediately before and after. In each case, when the temperatures were matched, values obtained for the mean and r.m.s. velocities were equivalent with and without dye injection.

3. Evaluation of detection algorithms

Results to be presented in this paper are based on a number of different experiments all of which were performed with the same nominal flow conditions, listed in table 2. That the flow was fully turbulent for these conditions was verified by making mean, r.m.s., and $\overline{uv}$ correlation measurements across the height of the channel w (see Bogard 1982). Profiles for each of these correspond well to previous measurements in fully turbulent channel flows by Kreplin & Eckelmann (1979), Hussain & Reynolds (1975), and Taslim *et al.* (1978).

Results based on direct comparison between flow visualization and velocity data were obtained from an experiment in which synchronized records were made for a period of 200 s. During this time the flow visualization indicated that 271 dye-marked events intersected the probe, of which 164 were identified as ejections. Comparisons between the flow visualization and the velocity-based detection algorithms were made in terms of these ejections rather than the whole burst structure for reasons to be discussed later.

3.1. *Detection algorithms*

Seven different detection algorithms were tested in this study including the three most widely used techniques: short-time autocorrelation; variable-interval time averaging

$\bar{U} = 0.129$ m/s (average velocity)	$Re_w = 8200$ $(\bar{U}w/\nu)$
$U_0 = 0.146$ m/s (centreline velocity)	$Re_\theta = 420$ $(U_0\theta/\nu)$
$w = 60$ mm (channel height)	$u_\tau = 0.79$ cm/s

TABLE 2. Experimental flow conditions

(VITA), and second-quadrant uv correlation. The following is a list of the detection algorithms along with associated parameters:

Autocorrelation, sample time T_s.
VITA, threshold ($k = \text{vâr}/\overline{u^2}$) and averaging time T_a.†
Quadrant, threshold ($H = -(uv)_2/u'v'$).‡
TPAV, smoothing window T_w.
U-level, threshold $L = -u/u'$.
Slope, threshold ($J = (\nu/u'u_\tau^2)\,\mathrm{d}u/\mathrm{d}t$) and smoothing window T_w.
VITA with slope, threshold ($k = \text{vâr}/\overline{u^2}$) and averaging time T_a.

Details of these techniques have been described previously in the literature as follows: Autocorrelation by Strickland & Simpson (1975), VITA by Blackwelder & Kaplan (1976), Quadrant by Lu & Willmarth (1973), TPAV by Wallace *et al.* (1977), U-level by Lu & Willmarth (1973), Slope by Simpson (1976) and VITA with slope by Johansson & Alfredsson (1982).

Two different methods were used to evaluate these detection algorithms. The first evaluation was in terms of the average time between events, which was compared to the correct values for $\bar{T}_B$ and the average time between ejections $\bar{T}_E$. A more thorough evaluation was possible for those techniques that detect discrete events, in which case one-to-one comparisons could be made with the ejections identified by flow visualization. This second comparison was possible for all the detection algorithms except the Autocorrelation method.

3.2. *Evaluation in terms of* $\bar{T}_B$

Both dye and hydrogen-bubble flow visualization have been used in the water-channel facility to determine $\bar{T}_B$ using the techniques described by Bogard & Tiederman (1983). Numerous measurements with the same nominal flow conditions have yielded a very repeatable value for $\bar{T}_B$ with a variation of less than $\pm 7\%$. Using these flow-visualization results as the standard, the measurement of $\bar{T}_B$ obtained by each of the burst-detection algorithms was evaluated. This is a very simple, but imprecise, way to test the accuracy of the various detection algorithms since a technique may count the right number of events but some of these events may not be bursts. However, since one of the major requirements of a burst-detection technique is to determine $\bar{T}_B$, this evaluation quickly identifies those techniques which have a serious deficiency.

Values of $\bar{T}_B$ obtained from each of the detection algorithms are given in figure 4, where they have been normalized with outer variables. For comparison, this figure also has values for both $\bar{T}_B$ and $\bar{T}_E$ obtained using flow visualization. Also noted on figure 4 are the results of four separate studies which were performed in the Max-Planck-Institut für Strömungsforschung oil channel with the same flow conditions.

† The overbar denotes a time-average value of the variable, and vâr is the variance of the streamwise velocity over a short integration time.

‡ The prime denotes the root-mean-square value of the variable.

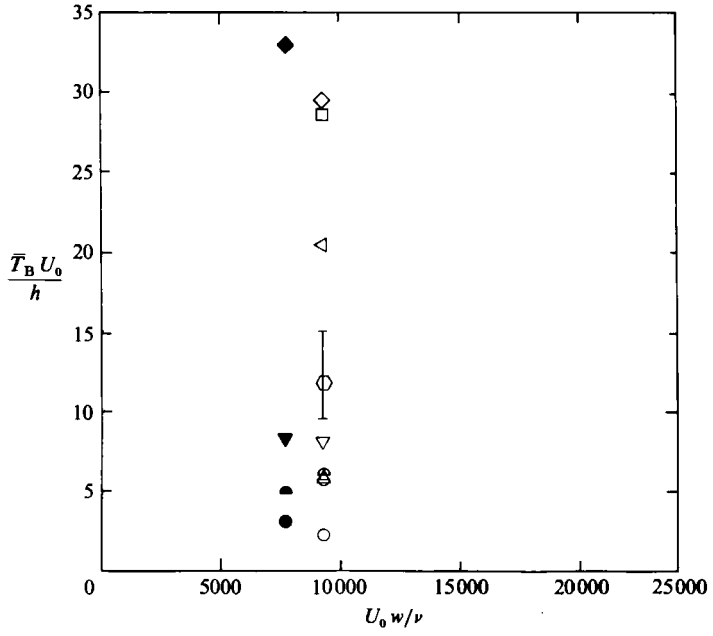

FIGURE 4. Average bursting periods using different detection algorithms: ◁, Narayanan & Marvin, Autocorrelation (1978); I, Strickland & Simpson, Autocorrelation (1975); ◇, Blackwelder & Eckelmann, VITA (1977); □, Lu & Willmarth, Quadrant (1973); ▽, Simpson, Positive slope (1976); ⌓, Wallace *et al.*, TPAV (1977); ⊂, Comte-Bellot *et al.*, Quadrant (1978); ○, Brodkey *et al.*, Quadrant (1974); ○, Present visual data, $\overline{T}_B$; △, Present visual data, $\overline{T}_E$. Open symbols; present measurements. Closed symbols; MPI oil-channel measurements.

Immediately apparent from figure 4 is the wide scatter in the results from both the present study and previous studies in the oil channel. However, each detection technique, which was originally used in the oil channel and later tested in the present study, yielded approximately the same normalized value for $\overline{T}_B$. The normalization used in figure 4 is in terms of outer variables U_0 and h, but essentially the same results are obtained using the variables u_τ and ν. Therefore each of these burst-detection algorithms has the positive attribute that the measurements are repeatable.

Most of the present results in figure 4 are based on the analysis of the same 200 s record of velocity data. The exceptions are the autocorrelation results which required significantly longer-time records. In order to duplicate the technique used by Narayanan & Marvin (1978) the autocorrelation was calculated from a velocity record of 1072 s. Following their technique, $\overline{T}_B$ was estimated as the second zero crossing of this autocorrelation and the result is shown on figure 4. To evaluate the autocorrelation techniques of Kim *et al.* (1971) and Strickland & Simpson (1975), a number of autocorrelations from shorter-time records were needed. Twelve records of 71.5 s, and six records of 179 s were used. The lengths of these records are equivalent to 30 and 70 average bursting periods respectively. Following the technique of Kim *et al.* (1971) and Strickland & Simpson (1975), $\overline{T}_B$ was estimated as the ensemble average of the time of the second peak on each of the autocorrelations. Values obtained were $\overline{T}_B = 1.93$ s based on the 71.5 s records and $\overline{T}_B = 3.10$ s based on the 179 s records. Because of this wide range depending on sample time, these results are depicted on figure 4 as a band covering the appropriate range.

As shown in figure 4, essentially all of the detection algorithms failed to measure

accurately the actual value of $\overline{T}_B$ as determined from flow-visualization results. Measurements range from a factor of 3 too large to a factor of 3 too small. The short-time autocorrelation technique of Strickland & Simpson (1975) is the only method which gave values reasonably close to the actual $\overline{T}_B$. However, as just shown, there was a large uncertainty associated with the measurement of $\overline{T}_B$ using the short-time autocorrelation technique.

3.3. *Direct comparison with individual ejections*

Two of the detection algorithms indicted an average time between events that corresponds well with the value for $\overline{T}_E$ determined from flow visualization. This might be expected since the signal characteristics used by the various detection algorithms are actually indications of a single, discrete event occurring at the probe. Hence these characteristics would be associated with each individual ejection passing the probe rather than with a series of ejections that compromise a single burst. Consequently the various detection algorithms are in fact best suited for the detection of the individual ejections. Direct comparisons between the flow visualization and the various detection algorithms was therefore done in terms of the individual ejections identified by each of these techniques.

To quantify the comparison between detected events and visualized ejections the probability that an ejection would be detected, and the probability of a false detection, were determined. A visualized ejection was said to have been detected by the probe if there was any overlap between the time periods of the ejection and one or more detected events. The probability of an ejection being detected $P(E)$ was then the ratio of the number of ejections detected to the total number of visually observed ejections. A false detection was said to have occurred if no part of the time period of an event identified by a detection algorithm overlapped with the time period of a visualized ejection. Thus, the probability of a false detection $P(E)$ was the ratio of the number of false detections to the total number of events indicated by the detection algorithm.

Results of the evaluation in terms of these probabilities are presented in table 3, where the parameters listed are those used in previous investigations. This evaluation indicates that only two of the detection algorithms, the Quadrant technique with a threshold of $H = 1.07$ and the U-level technique with a threshold of $L = 1.0$, have both a reasonably high probability of detecting an ejection and low probabilities of false detections. The Quadrant technique with a threshold of $H = 4$ and the VITA techniques have low probabilities of making false detections although a large percentage of the ejections are not detected. These latter results indicate that the thresholds were at levels such that only strong ejections were detected.

It was evident that in order to perform a thorough evaluation of the capabilities of each of the detection algorithms, comparisons should be made over a range of parameter values. For these comparisons, $P(F)$ values were determined as a function of the number of detections. These results are presented in figure 5. With the exception of the TPAV method, the number of detections for each algorithm is directly proportional to the threshold used. The number of detections for the TPAV method was set by adjustment of the smoothing-window parameter T_w'. For those algorithms which had a second adjustable parameter such as averaging times or smoothing windows, the optimum value for this parameter was determined by minimizing $P(F)$ while maintaining a constant number of detections of 164 by adjusting the thresholds. The number 164 corresponded to the number of ejections identified by flow visualizations during the sample time.

Detection algorithm	Parameters	$P(E)$	$P(F)$
Quadrant	$H = 4$	0.18	0.14
Quadrant	$H = 1.07$	0.69	0.15
Quadrant	$H = 0$	0.94	0.47
VITA	$k = 1.2$, $T_a^+ = 10$	0.09	0.18
VITA	$k = 1.0$, $T_a^+ = 14$	0.24	0.24
VITA with slope	$k = 1.0$, $T_a^+ = 10$	0.14	0.23
TPAV	$T_w^+ = 5$	0.82	0.65
U-level	$L = 1.0$	0.76	0.26
Positive slope	$J = 0.053$, $T_w^+ = 37$	0.37	0.46

TABLE 3. Evaluation of detection algorithms; probability than an ejection will be detected $P(E)$, and probability of a false detection $P(F)$

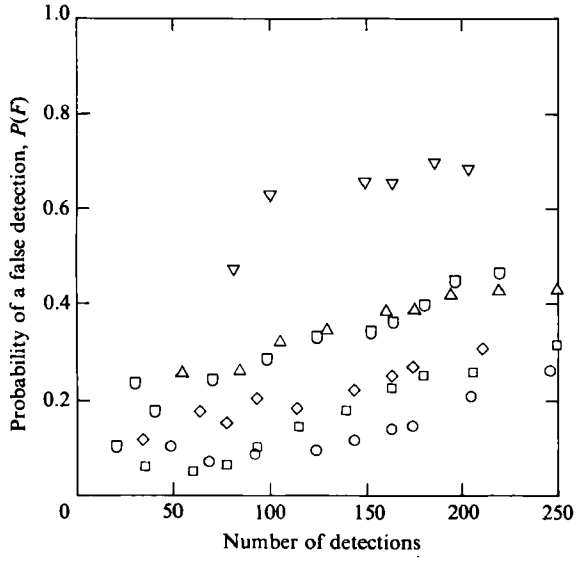

FIGURE 5. Probability of false detections as the number of detections during a 200 s sample time is varied by changing thresholds (TPAV detections varied by adjusting T_w): ○, Quadrant; □, U-level; ◇, VITA; △, positive slope; ▽, TPAV; ▢, VITA, with slope.

Most of the detection algorithms have a reasonably low probability of a false detection which decreases with the smaller number of detections obtained at higher thresholds. This result indicates that the detection algorithms are based on characteristics that are indeed associated with an actual ejection. As the number of detections become small the two best detection algorithms, the Quadrant and U-level techniques, reach minimum values of $P(F) \approx 0.07$. The continued occurrence of false detections at these high thresholds may be due partially to uncertainty in the flow visualization.

To have a reasonably high probability of detecting an ejection, the threshold for each detection algorithm must be set at a level to obtain approximately the same number of detections as the actual number of ejections occurring during the sample time. In this case the flow-visualization results indicate 164 ejections. For thresholds giving approximately 164 detections, the $P(F)$ value for the Quadrant technique, 14 %, was significantly less than for the U-level, 23 %, and VITA, 25 %, techniques.

Detection algorithm	Parameters
Quadrant	$H = 1.2$
VITA	$k = 0.64$, $T_a^+ = 26$
VITA with slope	$k = 0.35$, $T_a^+ = 10$
TPAV	$T_w^+ = 5$
U-level	$L = 1.3$
Positive slope	$J = 0.14$, $T_w^+ = 10$

TABLE 4. Threshold levels yielding the same number of detections as they visually determined number of ejections. Other parameters optimized for the minimum probability of a false detection.

Category	All	1	2	3	4	5	6
No. of ejections	164	37	49	32	10	17	19
Quadrant	0.65	0.97	0.76	0.66	0.40	0.41	0.05
U-level	0.63	0.86	0.76	0.66	0.40	0.47	0.11
VITA	0.60	0.81	0.67	0.56	0.40	0.47	0.32
VITA with slope	0.61	0.81	0.57	0.56	0.60	0.47	0.53
TPAV	0.82	0.84	0.90	0.75	0.80	0.71	0.79
Positive slope	0.60	0.86	0.57	0.53	0.60	0.41	0.42

TABLE 5. Probability of an ejection being detected $P(E)$. Parameters for each of the detection algorithms set at the values listed in table 4.

Threshold levels that give approximately 164 detections and optimum averaging times or smoothing times for the various detection algorithms are given in table 4. Using these parameters, each of the detection algorithms has been evaluated in terms of the probability of detecting an ejection $P(E)$, and these results are listed in table 5. Note that values for $P(E)$ have been determined for all ejections identified by the flow visualization, and for the specific ejection categories described in table 1. Based on all ejections, values for $P(E)$ are disappointingly low with a significant percentage of ejections apparently not detected. However, these results are misleading since they include ejections starting very close to the probe and that just barely touch it, and also ejections which begin far upstream of the probe and are far above the probe height as they pass the probe location. It is evident that a reasonable evaluation of the detection capabilities of the various algorithms must take into account the stage of development of the ejection when it is in contact with the probe.

Ejections in categories 1, 2, and 3 are respectively in the middle, late, and early stage of growth when they contact the probe. As seen in table 5, the probability of detecting these ejections is quite good. The Quadrant technique had the highest values for $P(E)$ in all three categories with the U-level technique matching these values in categories 2 and 3. The highest probability of detecting ejections was found for category 1 ejections, which are in the vigorous middle stage of growth. The Quadrant technique detected all but one of the 37 ejections in this category. Ejections in categories 4, 5, and 6 are all in a very late stage of growth. In category 4 the ejection appears to have ceased an active lifting away from the wall at the time when it contacts the probe. In both categories 5 and 6 the main body of the ejection passes above the probe with only a small tail which extends down to the wall actually contacting the probe. In category 5 this tail appears to be actively lifting away from the wall while in category 6 it does not. It should not be expected that the ejections

in these latter three categories would be readily detected by the probe and this is reflected in the low $P(E)$ values obtained for these categories. However, the failure to detect many of these ejections should not be viewed as a deficiency of the detection algorithms, but rather due to the difficulty of determining from the flow visualization if these latter-stage ejections are still active when they contact the probe. Ejections in the last three categories would have a good probability of being detected by a probe further upstream where the ejections would be in an earlier stage of development and closer to the wall.

Taken as a whole these results indicate that the Quadrant technique is a good detector of ejections. The less than perfect correlation can be attributed to the uncertainty in the flow-visualization analysis of determining which ejections were active and which had died out when making contact with the probe. Also, for ejections in early development, there was an uncertainty as to whether significant contact with the probe had been made. It is evident that when the ejection is still relatively active when contacting the probe, there is a good probability that it will be detected by the Quadrant technique.

Both the U-level and VITA algorithms appear to have a good probability of detecting ejections although they are less accurate than the Quadrant technique. The TPAV algorithm yields consistently high $P(E)$ values regardless of the ejection category. However, the TPAV algorithm indicates the detection of an event during a large percentage of the total time and therefore the technique will have a large probability of detecting an ejection just from random chance. The indiscriminate detection of ejections from different categories further suggests that detections for this technique are due to random probability.

Based on the results of these evaluations, the Quadrant technique was selected for further analysis because it is a valid detector of ejections with a high probability of detecting active ejections contacting the probe and a low probability of making false detections.

3.4. *Quadrant threshold*

In the previous section it was assumed that the appropriate threshold was that which would yield approximately the same number of ejections as identified by the flow visualization. Although this is a good first approximation, a more rigorous analysis is required to determine the sensitivity of the detection technique to the threshold used.

The threshold for the Quadrant technique is based on the level of the quadrant 2, $(uv)_2$, signal. For this analysis, the number of valid detections (i.e. detections that correspond to an ejection identified with flow visualization) was determined for detected events where the $(uv)_2$ signal was within a specified range. This threshold range ΔH was centred about various threshold levels H such that a detection was defined in terms of the $(uv)_2$ signal being within the following range:

$$H-\tfrac{1}{2}\Delta H \leqslant \frac{(uv)_2}{u'v'} \leqslant H+\tfrac{1}{2}\Delta H. \tag{1}$$

Results from this analysis are expressed in terms of the percentage of valid detections at each threshold level and are shown in figure 6. The threshold range used in this analysis was $\Delta H = 0.54$.

Shown in figure 6 are two data sets, file 8 and file 9, which represent separate records of velocity measurements at $y^+ = 15$. File 8 was the primary data set, recorded simultaneously with the flow visualization, and was therefore expected to have some correlation with visualized ejections. File 9 was recorded separately from the flow

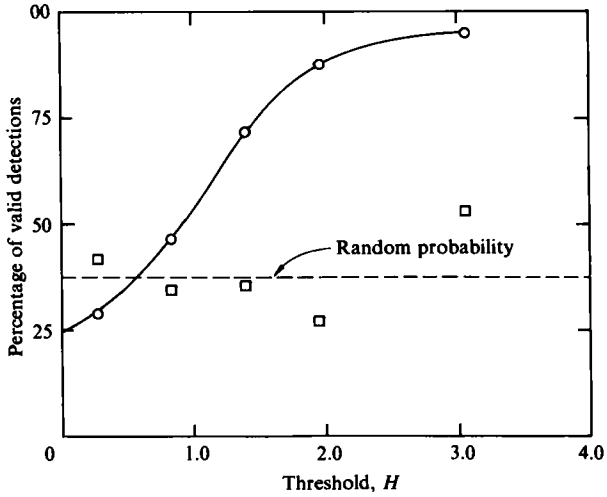

FIGURE 6. Percentage of valid detections using the Quadrant technique within a range $\Delta H = 0.54$ centred about threshold levels H: ○, file 8 (correlated); □, file 9 (uncorrelated).

visualization and therefore, when comparing events found from the analysis of this velocity data to the flow-visualization results, any correspondence between the two would be due only to random chance. The uncorrelated file 9 data was analysed as a check to determine the percentage of valid detections that would be obtained if there was in fact no real connection between the flow visualization and the velocity measurements.

The percentage of valid detections that would be obtained due to random probability can be estimated using the intermittency of the ejections and the duration of the detections. This random probability estimate is shown on figure 6 and is seen to be the approximate level of valid detections obtained with the uncorrelated data set. The scatter in the uncorrelated data can be attributed to the small number of samples, especially at the higher threshold levels.

For the correlated file 8 data, a significantly greater probability of having a valid detection is obtained for thresholds $H > 1$. Essentially, the maximum probability of having a valid detection is achieved at the level $H > 2$. The range of $1 < H < 2$ represents a region of transition from random detections to detections highly correlated with ejections. Since a large proportion of the detections made in this threshold range are valid detections of ejections, these results indicate that the appropriate threshold would be approximately $H = 1$. This threshold level would include the transition region and therefore would include a small percentage of apparently false detections.

Referring back to the three Quadrant threshold levels evaluated in table 3, we see that one of these, $H = 1.07$, is at the same level as indicated by the above analysis. This threshold level was obtained using the equations recommended by Comte-Bellot, Sabot & Saleh (1978):

$$H = \frac{|(\overline{uv})_2|}{u'v'}. \tag{2}$$

Since (2) sets the threshold at the average level of the second quadrant uv signal, Comte-Bellot *et al.* argue that it is a more accurate threshold than the low and high extremes used previously. Using this technique, Comte-Bellot *et al.* found that the

numerical value of the threshold level was $H \approx 1$ for a wide variation in Reynolds numbers, flow fields, and probe positions.

Using the threshold $H = 1.07$, a final evaluation of the Quadrant technique was done based on comparisons with ejections in the first five categories. Values of $P(E) = 0.77$ and $P(F) = 0.17$ were obtained from this analysis. Subsequent results presented in this paper were obtained using (2) for the threshold level.

4. Burst detection

The break-up of a streak can involve either a single ejection or multiple ejections which are closely grouped together. In previous investigations (Offen & Kline 1975 and Tiederman, Smith & Oldaker 1977) a distinction was made between ejections and the overall process of a streak break-up which was called a burst. Corino & Brodkey (1969) also observed groups of multiple ejections which 'appeared to be moving in a connected fashion', although they did not distinguish them as bursts. In a recent study using the VITA with slope-detection algorithms, Willmarth & Sharma (1984) found that they were measuring 'multiple bursts' which appeared to be part of the same burst event. Groups of multiple ejections also were observed frequently in the flow-visualization results obtained in the present study. In figure 7, which shows a histogram of the distribution of T_E obtained from the flow-visualization analysis, extreme skewness towards smaller values of T_E is an indication of the existence of groups of closely spaced ejections.

The skewed distributions of T_E in figure 7 is characteristic of an exponential distribution except for the lack of events occurring in the range $T_E < 0.2$ s. Physically, an exponential distribution would be expected if the ejections occurred at random intervals. The exponential distribution for the continuous variable T_E is analogous to the Poisson distribution for a discrete variable such as the number of events per unit time expected on a random basis. Since ejections have a finite duration, the distribution of T_E should not be expected to include many ejections separated by a time interval less than the mean duration of an ejection. To take this into account, the exponential distribution was modified to obtain a conditional probability distribution for randomly spaced events which are at least 0.2 s apart. This distibution is shown by the solid curve on figure 7. The good correspondence with the experimental data suggests that ejections are random events and not directly related to the low-velocity streaks. From this viewpoint the streak would act only as a passive source of dye to mark the ejection event. However, the following experiment has shown that this is not the case and that groups of ejections are related to the break-up of a single streak.

To determine if ejections are random events and independent of the streaks, a dye-slot flow-visualization experiment was performed in which ejections from the same streak, and from different streaks, were identified. This was accomplished by using two cameras to simultaneously record both plan and side views of the wall region. Histograms showing the temporal distribution of the number of ejections from the same streak and those from different streaks are given in figure 8. The interval between ejections from the same streak is seen to have a maximum of about 1.0 s, which is due to the finite length of the streaks. Ejections from different streaks have a minimum interval of approximately 0.6 s. The small percentage of ejections from different streaks in the interval from 0.5 to 1.0 s is significant. Assuming that ejections occur randomly and that there are no gaps in successive streaks, there would be a greater probability for ejections separated by an interval $T_E > 0.5$ s to come from

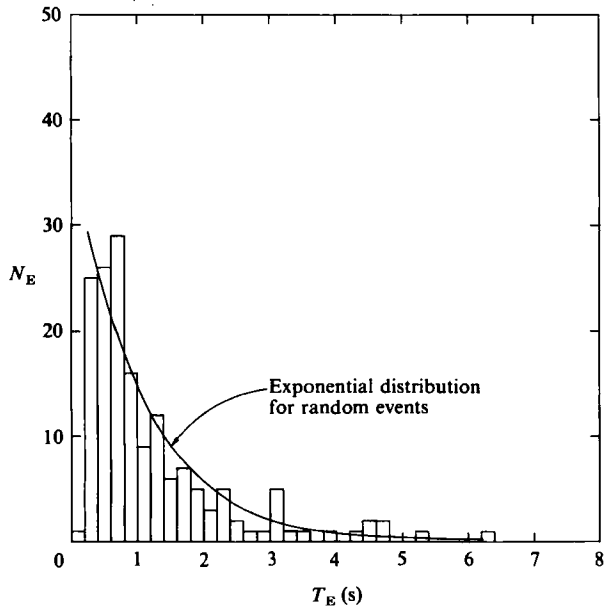

FIGURE 7. Histogram of the distribution of time between ejections T_E from visualization. Sample time 200 s; exponential distribution shown for comparison. File 8; number of visual ejections, 164; mean period 1.22 s.

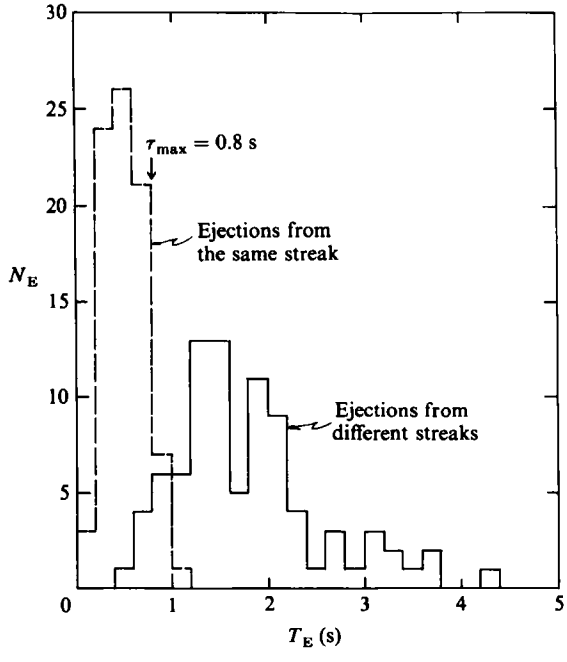

FIGURE 8. Histogram of the distribution of time between ejections T_E for ejections arising from the same and from different streaks. Based on 200 s sample time flow-visualization record.

different streaks than from the same streak. However, the experimental data contradict this, indicating that only 21 % of the ejections in the range $0.5 \leqslant T_E \leqslant 1.0$ s are from different streaks. Moreover, the results of Bogard & Tiederman (1983) showed that essentially all ejections that were identified with hydrogen bubbles were also identified with dye, indicating that no unmarked ejections occur in the gaps between streaks. Consequently, it must be concluded that ejections do not occur randomly, independent of the streaks. Rather the occurrence of a group of closely spaced ejections can be directly associated with the break-up of a single streak. Following the terminology of Kim *et al.* (1971), this event will be called a burst.

Using flow visualization, bursts can be distinguished easily with combined plan and side views as discussed previously. With probe measurements the only information available is the distribution of the time between ejections. From figure 8 it is evident that there is only a small overlap between the histograms of distributions of T_E from the same burst and T_E from different bursts. This suggests the possibility of distinguishing bursts by establishing an approximate maximum time between ejections τ_{max} such that ejections separated by less than τ_{max} would be from the same burst and those separated by more than τ_{max} would be from different bursts. From the data in figure 8 it can be seen that, for $\tau_{max} = 0.8$ s, 94 % of the ejections with $T_E < \tau_{max}$ are from the same burst. Therefore, once the value for τ_{max} has been determined it can be used to obtain a reasonable approximation of which ejections are from the same burst.

The histogram of the distribution of T_E obtained by using the Quadrant technique to detect ejections is given in figure 9. These data are based on the analysis of a 200 s velocity record taken simultaneously with the flow visualization used to obtain figure 7. The distribution of T_E obtained with probe measurements is very similar to the flow-visualization results of figures 7 and 8. However, there is a marked increase in the number of ejections in the interval $T_E < 0.4$ s. This is probably due to probe detections having better resolution than the flow visualization and therefore being better able to discern two ejections that are very close together. The histogram in figure 9 does indicate a bimodal distribution with a gap at $T_E = 0.8$ s, which corresponds to the value for τ_{max} determined previously. Analysis of a second velocity-data file did not produce a bimodal distribution that is as distinct as figure 9. Therefore, visual inspection of a histogram is not a reliable method for determining a value for τ_{max}.

In figure 10 the probability distribution function for the experimental data is compared with an exponential distribution function modified for the condition that $T_E \geqslant T_0$. Thus the modified exponential distribution is a conditional probability function for random events which occur with an interval between events that is always greater than T_0. The T_0 value accounts for the finite duration of the ejections during which time it is not possible to detect a second ejection. For the present results a value of $T_0 = 0.094$ s was used, which corresponds to the mean duration of ejections detected by the Quadrant technique at $y^+ = 15$. The average time between ejections was used to obtain the normalized form of the parameter used in the exponential function.

For both velocity samples taken at $y^+ = 15$, figure 10 shows that the distribution follows an exponential distribution at larger values of T_E, but there is a definite deviation from the exponential distribution at low values of T_E. In both cases the experimental probability distribution functions had a larger number of events when the exponential function was less than 0.5. This corresponds to $T_E < 0.8$ s and is consistent with the flow-visualization results, which indicated the intersection of two

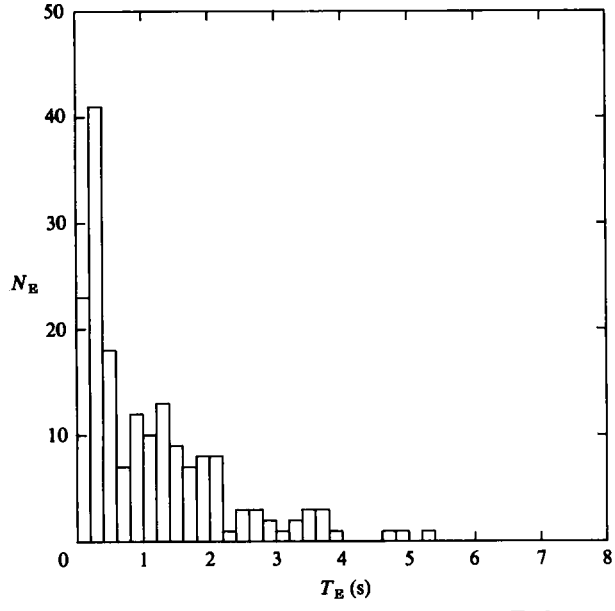

FIGURE 9. Histogram of the distribution of time between ejections T_E from velocity measurements using the Quadrant technique. Measurements at $y^+ = 15$; sample time of 200 s. File 8; 179 *uv* detections; threshold $H = 1.068$; mean period 1.13 s.

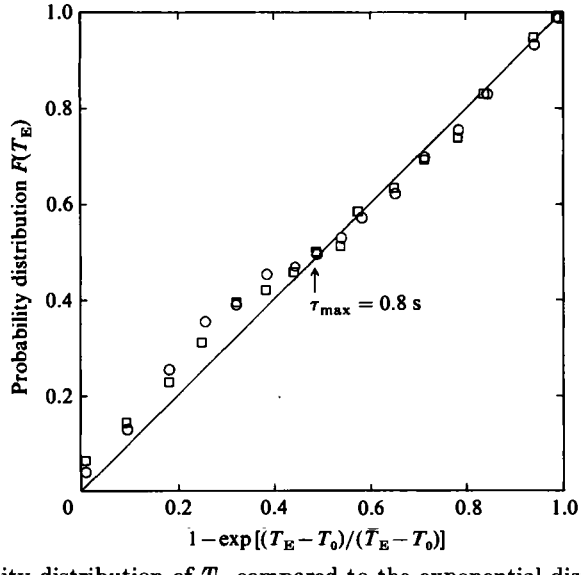

FIGURE 10. Probability distribution of T_E compared to the exponential distribution for $T_E \geqslant T_0$. Ejections detected with velocity measurements analysed using the Quadrant technique. $y^+ = 15$; ○, file 8; □, file 9.

different distributions for ejections at this point. Therefore the maximum time between ejections from the same burst τ_{max} can be determined from the distribution of T_E values obtained using the Quadrant technique when the information is plotted in the form shown in figure 10.

Once the value of τ_{max} has been determined, ejections separated by times less

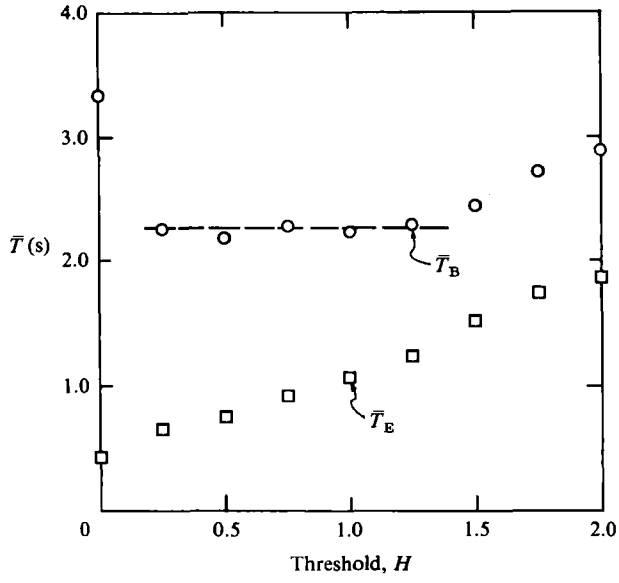

FIGURE 11. Average burst and ejection periods as a function of threshold using Quadrant technique for detecting ejections. $y^+ = 15$.

than τ_{max} can be grouped into single bursts. Using this technique, ejections detected with the Quadrant technique were grouped into bursts and the average time between bursts was determined for a range of thresholds. For this evaluation, τ_{max} was held constant at the previously determined value of $\tau_{max} = 0.8$ s. Resulting values for $\bar{T}_B$ and $\bar{T}_E$ are presented in figure 11. Although $\bar{T}_E$ systematically increased as threshold level was increased, $\bar{T}_B$ remained constant from a very low threshold to a threshold slightly greater than $H = 1.0$. This result was somewhat surprising considering the results presented in figure 6, which indicated that ejections detected at thresholds less than $H = 1.0$ were little more than random events. In figure 12 the probability distribution function for ejections detected at various thresholds is compared with the exponential distribution expected for random events. At the lowest threshold, $H = 0.25$, the data are significantly closer to the exponential distribution. This indicates that the additional events detected at lower thresholds have a random distribution. Therefore, the number of bursts detected remains relatively constant even though the additional 'ejections' detected at lower thresholds are random events unrelated to the bursting process. Based on the criterion used to identify bursts, a random event may have the effect of increasing, decreasing, or not changing the number of bursts indicated. For the present case the random events detected at lower thresholds have an equal probability of increasing or decreasing the number of bursts. The net effect is an insensitivity to these random events resulting in a relatively constant measure of $\bar{T}_B$.

The Quadrant technique was used to analyse velocity data taken at various positions across the channel height. Equation (2) was used to determine thresholds ranging in value from $H = 0.9$ to 1.3. Values for $\bar{T}_E$ are presented in figure 13. These data indicate a rapid increase in the number of ejections up to $y^+ = 50$. The maximum number of ejections occurred at $y^+ = 100$ and slowly decreased from that point towards the centreline of the channel.

The probability distribution function of T_E is given in figure 14 for three different

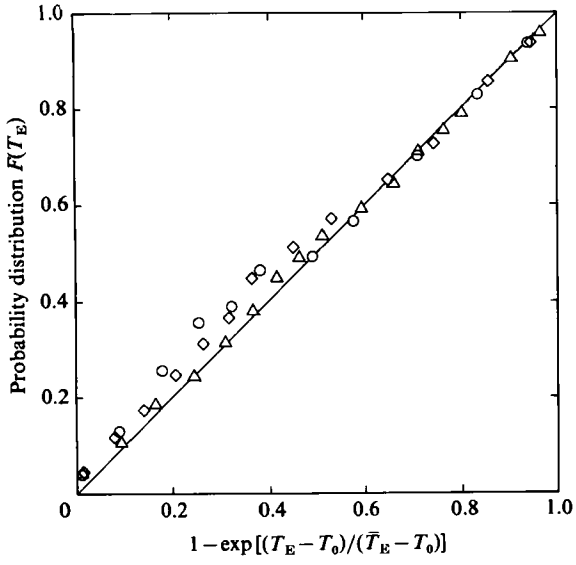

FIGURE 12. Probability distribution of T_E for different threshold levels using the Quadrant technique. $y^+ = 15$; ○, $H = 1.07$; ◇, 0.50; △, 0.25.

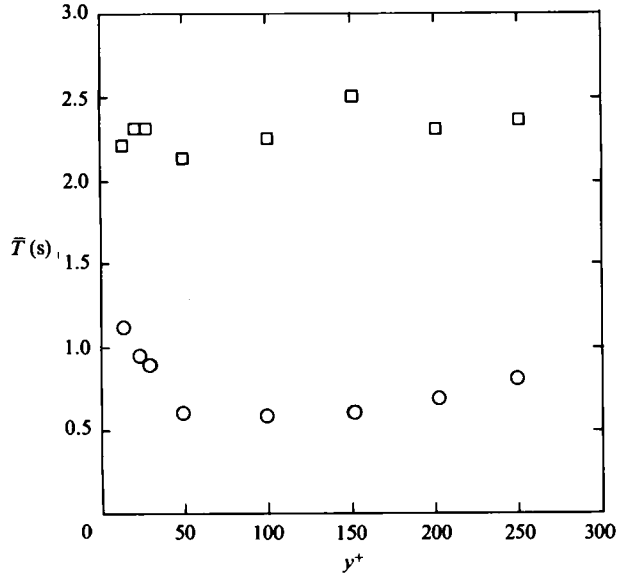

FIGURE 13. Average burst and ejection period at increasing distances from the wall. Ejections detected using the Quadrant technique with threshold from (2). □, $\bar{T}_B$; ○, $\bar{T}_E$.

distances from the wall, $y^+ = 15$, 30, and 101. Again these distributions are compared with an exponential distribution and the actual probability distribution is found to be significantly larger than exponential distribution for low values of T_E. Although the number of ejections increased by a factor of more than two at $y^+ = 101$, the deviation from the exponential distribution becomes more pronounced. This result indicates that the additional ejections detected at larger distances from the wall were

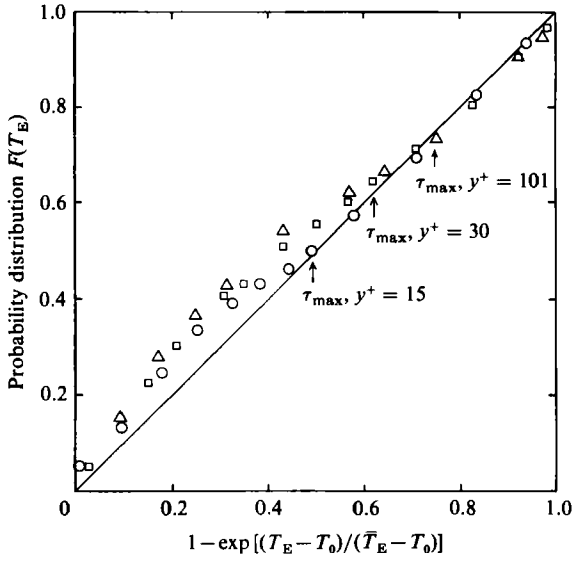

FIGURE 14. Probability distribution of T_E for increasing distances from the wall. Ejections detected using the Quadrant technique with threshold from (2). ○, $y^+ = 15$; □, 30; △, 101.

not randomly distributed, but occurred relatively close to existing ejections and thereby increased the probability for events at small values of T_E.

At all y^+ locations the deviation from the exponential distribution occurred at approximately $T_E = 0.8$ s. Consequently this value was used for τ_{max} to identify bursts at varying distances from the wall. The results, presented in figure 13, show that $\bar{T}_B$ remained essentially constant across the channel height. Therefore the number of bursts remained the same at different probe positions although the number of ejections increased substantially. Consequently, the number of ejections in a burst increased as the burst moved away from the wall.

An explanation for this is found in the nature of the fluid element that forms an ejection. From the comparisons with flow visualization it was evident that the high $(uv)_2$ signal detected with the Quadrant technique was due to the low-speed fluid of a streak being ejected into the outer regions of the flow. The streak is a long, narrow filament of fluid which becomes very contorted as it is ejected away from the wall. An ejection is detected by the probe each time a segment of this filament intersects the probe. As the streak filament breaks up when it moves away from the wall it becomes more contorted, so that a larger number of filament segments cross the probe position. Since the increased number of ejections is due to the break-up of a streak filament, which formed one ejection near the wall, into multiple ejections far from the wall, we expect that the new ejections will tend to be very close together and of shorter duration. This was confirmed by the experimental data, which showed that, although the total number of ejections increased by a factor of two when moving from $y^+ = 15$ to 101, the number of ejections occurring within $T_E = 0.2$ s increased by a factor of six. The average duration of these ejections decreases from 0.094 to 0.051 s.

5. Conclusion

The major conclusion of this study is that the Quadrant technique applied to single-point velocity measurements can detect bursts. This is due to the high $(uv)_2$ signal which is uniquely associated with the ejections that form bursts. With the appropriate threshold, this signal can identify ejections and the ejections can be grouped into bursts using a period discrimination determined by comparing the experimental results to a random process.

The optimum threshold for the Quadrant technique was determined by direct comparison with flow visualization and was found to be $H \approx 1.0$. This threshold level is predicted by the equation suggested by Comte-Bellot *et al.* (1978) based on the average level of the $(uv)_2$ signal. Based on comparisons with visualized ejections from categories 1–5, the Quadrant technique had a probability of detecting an ejection of $P(E) = 77\,\%$, and a probability of making a false detection of $P(F) = 17\,\%$. The probability of detecting an ejection was dependent on the certainty with which the flow visualization indicated the ejection was active when it contacted the probe. The probability of detecting an ejection approached 100 % for those that were the most active ejections. We conclude from these results that the correlation between ejections detected with the Quadrant technique and visualized ejections is as high as would reasonably be expected considering the difficulties of precisely interpreting flow visualization.

Other algorithms, VITA and U-level, have a low probability of making a false detection of an ejection when high thresholds are used. However, when thresholds are lowered in order to detect all ejections, these techniques are significantly less accurate than the Quadrant technique.

An order-of-magnitude variation in the value of $\overline{T}_B$ was obtained when using various burst-detection techniques presented in the literature. These discrepancies are due to the inaccuracies of the detection algorithms and/or the threshold levels used with these algorithms. Only the short-time autocorrelation technique achieved reasonable correspondence with the bursting rate obtained by flow visualization. However, there was a large variance in the values of $\overline{T}_B$ from one sample to the next when using this technique.

The detection algorithms designed to detect individual events are generally based on a particular velocity characteristic associated with a single ejection. However, generally no distinction has been made between ejections and bursts for any of these techniques as described in the literature. In the present study it was confirmed that the burst process is an identifiable event which may involve multiple ejections coming from the same streak. The importance of identifying bursts was demonstrated when analysing velocity data at varying distances from the wall. Here it was seen that the number of ejections increased dramatically as the streak broke up when it moved away from the wall. However, the number of bursts remained constant at the different probe positions.

Identification of bursts using the Quadrant technique is accomplished by establishing a value for the maximum time between ejections from the same burst τ_{max}. Using the distribution of T_E obtained with the velocity measurements, the value for τ_{max} can be determined as the point where the actual distribution function deviates from the exponential distribution function expected for random events. From flow-visualization results it was determined that there is a 94 % probability that ejections are from the same burst if $T_E < \tau_{max}$. Furthermore, when using this procedure to identify bursts in conjunction with the Quadrant technique, values for $\overline{T}_B$ were obtained that were independent of threshold over the range $H = 0.25$ to 1.25.

REFERENCES

ACHIA, B. U. & THOMPSON, D. W. 1977 Structure of the turbulent boundary layer in drag-reducing pipe flow. *J. Fluid Mech.* **81**, 439.

ALFREDSSON, P. H. & JOHANSSON, A. Y. 1984 Timescales in turbulent channel flow. *Phys. Fluids* **27**, 1974.

BLACKWELDER, R. F. & ECKELMANN, H. 1977 The spanwise structure of the bursting phenomenon. *Rep. No.* 121/1977, MPI Strömungsforschung, Göttingen.

BLACKWELDER, R. F. & HARITONIDIS, J. H. 1983 Scaling of the burst frequency in turbulent boundary layers. *J. Fluid Mech.* **132**, 87.

BLACKWELDER, R. F. & KAPLAN, R. E. 1976 On the bursting phenomenon near the wall in bounded turbulent shear flows. *J. Fluid Mech.* **76**, 89.

BOGARD, D. G. 1982 Investigation of burst structures in turbulent channel flows through simultaneous flow visualization and velocity measurements. Ph.D. thesis, Purdue University.

BOGARD, D. G. & TIEDERMAN, W. G. 1983 Investigation of flow visualization techniques for detecting turbulent bursts. *Symposium on Turbulence 1981*, p. 289. University of Missouri-Rolla.

BRODKEY, R. S., WALLACE, J. M. & ECKELMANN, H. 1974 Some properties of truncated turbulence signals in bounded shear flows. *J. Fluid Mech.* **63**, 209.

CHEN, C. P. & BLACKWELDER, R. F. 1978 The large-scale motion in a turbulent boundary layer: a study using temperature contamination. *J. Fluid Mech.* **89**, 1.

COMTE-BELLOT, G., SABOT, J. & SALEH, I. 1978 Detection of intermittent events maintaining Reynolds stress. In *Proc. Dynamic Flow Conf. – Dynamic Measurements in Unsteady Flows*, p. 213. Marseille.

CORINO, E. R. & BRODKEY, R. S. 1969 A visual study of turbulent shear flow. *J. Fluid Mech.* **37**, 1.

DONOHUE, G. L., TIEDERMAN, W. G. & REISCHMAN, M. M. 1972 Flow visualization of the near-wall region in a drag-reducing channel flow. *J. Fluid Mech.* **56**, 559.

ECKELMANN, H. 1974 The structure of the viscous sublayer and the adjacent wall region in a turbulent channel flow. *J. Fluid Mech.* **65**, 439.

GRASS, A. J. 1971 Structural features of turbulent flow over smooth and rough boundaries. *J. Fluid Mech.* **50**, 223.

HEIDRICK, T. R., BANERJEE, S. & AZAD, R. S. 1977 Experiments on the structure of turbulence in fully developed pipe flow. 2. A statistical procedure for identifying 'burst' in the wall layers and some characteristics of flow during bursting periods. *J. Fluid Mech.* **82**, 705.

HUSSAIN, A. K. M. F. & REYNOLDS, W. C. 1975 Measurements in fully developed turbulent channel flow. *Trans. ASME* I: *J. Fluids Engng* **97**, 568.

JOHANSSON, A. V. & ALFREDSSON, P. H. 1982 On the structure of turbulent channel flow. *J. Fluid Mech.* **122**, 295.

KASAGI, N. & HIRATA, M. 1976 'Bursting phenomena' in turbulent boundary layer on a horizontal flat plate heated from below. In *Heat Transfer and Turbulent Buoyant Convection* (ed. E. B. Spalding & N. Afgan), vol. 1, p. 27. Hemisphere.

KIM, H. T., KLINE, S. J. & REYNOLDS, W. C. 1971 The production of turbulence near a smooth wall in a turbulent boundary layer. *J. Fluid Mech.* **50**, 133.

KLINE, S. J., REYNOLDS, W. C., SCHRAUB, F. A. & RUNSTADLER, P. W. 1967 The structure of turbulent boundary layer. *J. Fluid Mech.* **30**, 741.

KREPLIN, H. & ECKELMANN, H. 1979 Behavior of the three fluctuating velocity components in the wall region of a turbulent channel flow. *Phys. Fluids* **22**, 1233.

LAUFER, J. & NARAYANAN, M. A. B. 1971 Mean period of the turbulent production mechanism in a boundary layer. *Phys. Fluids* **14**, 182.

LU, S. S. & WILLMARTH, W. W. 1973 Measurement of structure of the Reynolds stress in a turbulent boundary layer. *J. Fluid Mech.* **60**, 481.

MIZUSHINA, T. & USUI, H. 1977 Reduction of eddy diffusion for momentum and heat in viscoelastic fluid flow in a circular tube. *Phys. Fluids Suppl.* **20**, S100.

NARAYANAN, B. & MARVIN, J. 1978 On the period of the coherent structure in boundary layers at large Reynolds numbers. In *Proc. of the Workshop on Coherent Structure in Turbulent Boundary Layers*, p. 380. Lehigh University, Bethlehem, Penn.

NAKAGAWA, H. & NEZU, I. 1981 Structure of space–time correlations of bursting phenomena in an open-channel flow. *J. Fluid Mech.* **104**, 1.

OFFEN, G. R. & KLINE, S. J. 1975 A comparison and analysis of detection methods for the measurements of production in a boundary layer. In *Proc. 3rd Biennial Symposium of Turbulence in Liquids*, p. 289. University of Missouri-Rolla.

RAO, K. N., NARASIMHA, R. & BADRI NARAYANAN, M. A. 1971 The bursting phenomenon in a turbulent boundary layer. *J. Fluid Mech.* **48**, 339.

RAUPACH, M. R. 1981 Conditional statistics of Reynolds stress in rough-wall and smooth-wall turbulent boundary layers. *J. Fluid Mech.* **108**, 363.

SABOT, J. & COMTE-BELLOT, G. 1976 Intermittency of coherent structures in the core region of fully developed turbulent pipe flow. *J. Fluid Mech.* **74**, 767.

SIMPSON, R. L. 1976 An investigation of the spatial structure of the viscous sublayer. *Rep. No. 188*, MPI Strömungs forschung, Göttingen.

SMITH, C. R. 1978 Visualization of turbulent boundary-layer structure using a moving hydrogen bubble-wire probe. In *Proc. of the Workshop on Coherent Structure of Turbulent Boundary Layers*, p. 340. Lehigh University, Bethlehem, Pennsylvania.

STRICKLAND, J. H. & SIMPSON, R. L. 1975 'Bursting' frequencies obtained from wall shear stress fluctuations in a turbulent boundary layer. *Phys. Fluids* **18**, 306.

TASLIM, M. E., KLINE, S. J. & MOFFAT, R. J. 1978 Calibration of hot-wires and hot-films for velocity fluctuations. *Rep. TMC-4*, Stanford University.

TIEDERMAN, W. G., SMITH, A. J. & OLDAKER, D. K. 1977 Structure of the viscous sublayer in drag-reducing channel flows. In *Proc. of the 4th Biennial Symposium on Turbulence in Liquids*, p. 312. University of Missouri-Rolla.

UEDA, H. & MIZUSHINA, T. 1979 Turbulence structure in the inner part of the wall region in a fully developed turbulent tube flow. In *Proc. of the 5th Biennial Symposium on Turbulence*, p. 357. Science Press, Princeton.

WALLACE, J. M., BRODKEY, R. S. & ECKELMANN, H. 1977 Pattern-recognized structures in bounded turbulent shear flows. *J. Fluid Mech.* **142**, 121.

ZAKKAY, V., BARRA, V. & WANG, C. R. 1978 The nature of boundary layer turbulence at high subsonic speeds. *AIAA Paper No.* 78–198.